Ocean Modelling 139 (2019) 101399

Contents lists available at ScienceDirect

Ocean Modelling

journal homepage: www.elsevier.com/locate/ocemod

The impact of ocean surface currents on global eddy kinetic energy via the wind stress formulation

Zhitao Yu*, E. Joseph Metzger

Naval Research Laboratory, Stennis Space Center, MS, USA

A B S T R A C T

A pair of 12.5-year (July 2002–December 2014) HYbrid Coordinate Ocean Model (HYCOM) simulations that only differ in the wind stress formulation are used to investigate the effect of ocean surface currents on global monthly eddy kinetic energy (EKE) variation. The model results (2004–2014) show that the global monthly mean EKE is reduced by 37%, from 1.76 EJ (10^{18} J) to 1.10 EJ after ocean surface currents are included in the wind stress formulation. The monthly EKE budget indicates that the shear production and buoyancy work are positive (energy source) and the eddy wind work on the geostrophic currents is negative (energy sink) in the steady state (2004–2014) for both simulations. All of these three terms are reduced in the steady state when the ocean currents are included in the wind stress formulation. The global integral of the EKE difference budget suggests that the EKE reduction is primarily due to the reduction of the buoyancy work, followed by the reduction of the wind work on the geostrophic currents and the shear production. To our knowledge this is the first study to separate the eddy wind work into the geostrophic and ageostrophic components to investigate the impact of ocean surface currents on global and depth integrated EKE via the wind stress formulation using HYCOM simulations.

1. Introduction

The global ocean circulation can be divided into two parts: the time mean flow and an eddy component relative to the time mean flow. The global ocean kinetic energy can also be divided into two parts: one associated with the time mean flow and the other being the eddy component. The eddy kinetic energy (EKE) of the global ocean circulation is important to measure and map because it is much larger than the time mean kinetic energy and is thought to be driving the mean circulation in some high eddy activity regions (Holland et al., 1983; Richardson, 1983). The EKE is mainly contained by mesoscale eddies, meanders, and rings of the boundary currents and is generated by instabilities of the mean flow and direct surface wind forcing (Stammer, 1997; Ferrari and Wunsch, 2009, 2010), which is clearly demonstrated by the domain integral of the EKE budget (Hughes et al., 2009) as shown below in tensor notation following the standard Reynold decomposition,

$$\frac{\partial(EKE)}{\partial t} = SP + BW + \varepsilon, \tag{1}$$

where

$$EKE = \frac{\rho_o}{2}\int_V \overline{u_i'^2}dV, \tag{2}$$

$$SP = -\rho_o \int_V \overline{u_i' u_j'}\frac{\partial \overline{u_j}}{\partial x_i}dV, \tag{3}$$

$$BW = -g\int_V \overline{\rho' w'}dV. \tag{4}$$

Here u_i are the components of the velocity vector $\boldsymbol{u}$, ρ_o is the density of sea water, V is the volume of the global ocean, x_i are the spatial coordinates, g is the gravitational constant, ρ is the Boussinesq density, and $w = u_3$ is the vertical velocity. Terms with an overbar denote the time average of the variable (mean flow) and terms with a prime indicate fluctuations (eddy components) relative to the corresponding time average, this implies that $\overline{u_i'} = 0$. The advection of EKE by the mean flow and the eddy transfer of EKE terms vanish in the domain integral as they only move EKE around inside of the global ocean.

There are three terms contributing to the changes of EKE, *SP*, *BW*, and ε. *SP*, the shear production, contains nine terms and represents how eddy motions extract kinetic energy from the mean flow through barotropic and Kelvin-Helmholtz instabilities. *BW*, the buoyancy work, represents how available potential energy in the mean flow converts into EKE through baroclinic instability. The third term in the r.h.s. of Eq. (1), ε, describes the dissipative processes through sub-grid scale turbulence and has a general form of

$$\varepsilon = \rho_o \nu \int_S \overline{u_i'\frac{\partial u_i'}{\partial x_j}}n_j dS - \rho_o \nu \int_V \overline{\left(\frac{\partial u_i'}{\partial x_j}\right)^2}dV, \tag{5}$$

* Corresponding author at: Oceanography Division, Naval Research Laboratory, Stennis Space Center, MS 39529, USA.
E-mail address: zhitao.yu@nrlssc.navy.mil (Z. Yu).

https://doi.org/10.1016/j.ocemod.2019.05.003
Received 25 October 2018; Received in revised form 1 May 2019; Accepted 12 May 2019
Available online 17 May 2019
1463-5003/ Published by Elsevier Ltd.

after applying surface boundary conditions of no normal flow. Here ν is the turbulence viscosity and S is the ocean surface bounding V with unit normal n_j. Please note that Eq. (5) is simplified by assuming ν is constant. In our numerical simulations, ν is calculated from the K-profile parameterization model and is space and time dependent. Since there are no tides in this study, we can simplify (Kuhlbrodt et al., 2007; Hughes et al., 2009) Eq. (5) to

$$\varepsilon = \int_S \overline{\tau' \cdot V_o'} dS + td, \tag{6}$$

where, $\boldsymbol{\tau}$ is the wind stress vector and $\boldsymbol{V}_o$ is the ocean surface current. The first r.h.s. term of Eq. (6) is the eddy wind work ($\overline{\tau' \cdot V_o'} dS$) on the ocean surface and the second term, $td = -\rho_o \nu \int_V \overline{\left(\frac{\partial u_i'}{\partial x_j}\right)^2} dV$, is the sub-surface dissipation in the global ocean except at the surface. Please note that td contains both the global interior turbulence dissipation and the bottom friction. Since the turbulence viscosity (ν, which depends on both the resolved shear instability and unresolved shear instability due to the background internal wave field) was not saved in our numerical simulations, we can only estimate td as a residual from Eq. (1) as shown in section 3.4.

In order to obtain the time evolution of EKE, the overbar is defined as the monthly average that eliminates the fluctuations while still permitting slow seasonal variations of the mean flow. Please note that if the overbar terms are calculated as the long-term time average, Eq. (1) would become $0 = SP + BW + \varepsilon$. Hereafter, the kinetic energy associated with eddy flow relative to mean flow is referred to as variability kinetic energy (VKE, Wunsch, 1998) and the EKE is referred to as the kinetic energy associated with eddy flow relative to the monthly mean.

In the last two decades, there are many studies investigating wind stress dependence on the ocean surface currents. A new wind stress formulation,

$$\tau = \rho_a C_d \, |\boldsymbol{V}_{10} - \boldsymbol{V}_o| (\boldsymbol{V}_{10} - \boldsymbol{V}_o), \tag{7}$$

has been shown to be more appropriate than the commonly used wind stress formulation,

$$\tau = \rho_a C_d \, |\boldsymbol{V}_{10}| \, \boldsymbol{V}_{10}, \tag{8}$$

that assumes $\boldsymbol{V}_o$ in Eq. (7) to be zero. Here $\rho_a$is the air density, $C_d$is the drag coefficient, and $\boldsymbol{V}_{10}$ is the 10-m atmospheric wind. This new wind stress formulation improves ocean numerical simulations (Pacanowski, 1987; Luo et al., 2005; Renault et al., 2016b; Yu et al., 2017), reduces ocean surface momentum and heat fluxes (Kelly et al., 2001; Dawe and Thompson, 2006) and surface wind work (Dawe and Thompson, 2006; Duhaut and Straub, 2006; Zhai and Greatbatch, 2007; Hughes and Wilson, 2008; Xu and Scott, 2008), and also reduces Sverdrup transport in the mid-latitude (Yu et al., 2017). Furthermore, it was shown that the new wind stress formulation reduces surface EKE by 10 to 50% (Zhai and Greatbatch, 2007; Eden and Dietze, 2009; Seo et al., 2016; Renault et al., 2016a; Renault et al., 2016b) in different regions of global ocean. Renault et al. (2016a) also found that the new wind stress formulation reduces the depth-integrated EKE by 27% in the California Upwelling System.

There are two pathways, direct and indirect, via which the EKE can be affected by the wind stress formulation (Eden and Dietze, 2009). The direct pathway is the eddy wind work, the first term in Eq. (6), while the indirect pathway refers to the changes of SP and BW in Eq. (1) and td in Eq. (6) due to the changes of the mean circulation generated by the new wind stress formulation. To explain the reduction of surface EKE due to the wind stress dependence on the ocean surface currents, Eden and Dietze (2009) analyzed the EKE budget in the upper 50 m for their North Atlantic model outputs and Seo et al. (2016) applied the EKE budget to their numerical results in the California Current System. Both of these studies suggested that the surface EKE reduction is primarily due to the reduced eddy wind work because the reduction of SP and BW is much smaller.

The ocean surface current, $\boldsymbol{V}_o$, in Eq. (7) can be split into geostrophic ($\boldsymbol{V}_g$) and ageostrophic ($\boldsymbol{V}_{ag}$) components. Thus, the eddy wind work input into the global ocean circulation contains both eddy wind work on surface geostrophic currents and ageostrophic currents,

$$\overline{\tau' \cdot V_o'} = \overline{\tau' \bullet V_g'} + \overline{\tau' \bullet V_{ag}'}. \tag{9}$$

The classical theory states that the wind work on ageostrophic currents is fully dissipated through the vertical turbulent dissipation to maintain the Ekman spiral in the Ekman layer (Wang and Huang, 2004). Wunsch (1998) stated that wind work on Ekman-like flow is dissipated within the surface mixed layer and does not directly produce any motions included in the general circulation per se. The global eddy wind work on ageostrophic currents is estimated to be 4.15 TW (Yu et al., 2018), much larger than the estimate of the global eddy wind work on geostrophic currents, from −0.099 (Yu et al., 2018) to 0.009 (Hughes and Wilson, 2008), and 0.039 TW (Wunsch, 1998). Thus, comparing eddy wind work $\overline{\tau' \cdot V_o'} dS$ with SP and BW greatly overlooks the impact of SP and BW and overestimates the effect of eddy wind work on the EKE variation.

In this study, we perform the global EKE budget analysis using model output from two global HYbrid Coordinate Ocean Model (HYCOM) simulations to reveal why the global EKE integral is reduced by the wind stress dependence of the ocean surface currents. This research differs and improves on previous work in that (1) it studies the depth-integrated EKE instead of the upper ocean EKE and thus, (2) it compares eddy wind work on geostrophic currents in Eq. (9), instead of eddy wind work $\overline{\tau' \cdot V_o'} dS$, with SP and BW. And note also that this study is based on results from global HYCOM instead of regional model on z (Eden and Dietze, 2009) or terrain-following vertical levels (Seo et al., 2016). To our knowledge this is the first study to separate the eddy wind work into the geostrophic and ageostrophic components to investigate the impact of ocean surface currents on global and depth integrated EKE via the wind stress formulation using HYCOM simulations. This paper is organized as follows: Section 2 describes the numerical model and experimental configuration. Model results are presented and analyzed in section 3, which is followed by discussion and conclusions in section 4.

2. Numerical simulations

The two global numerical simulations are performed with HYCOM, a widely used primitive equation general ocean circulation model. A detailed description of HYCOM physics was given by Bleck (2002). There is no data assimilation applied to the numerical model in this study. There are also no tides or surface waves effect in the simulations either. The two HYCOM global simulations differ only in the wind stress formulation. Experiment 1 does not include the effect of ocean surface currents in the wind stress formulation (Eq. (8)) whereas experiment 2 does (Eq. (7)). Below, HYCOM is briefly presented with emphasis on the numerical aspects that are relevant to this study.

The HYCOM horizontal resolution in this study is 0.08° (1/12.5°): ~9 km at the equator and ~6.5 km at mid-latitudes. The grid is uniform cylindrical from 78.64°S - 66°S, Mercator between 66°S - 47°N and includes a bipolar patch north of 47°N providing ~3.5 km grid spacing at the North Pole. There are 41 hybrid coordinate layers (z, sigma, and isopycnal) vertically with potential density referenced to 2000 m. The top vertical layer has a uniform layer thickness of 1 m.

The initialization state for the two simulations is obtained in a two-step process: 1) a global HYCOM simulation is forced (according to Eq. (8)) by a 1993–2012 surface forcing climatology obtained from the 0.3125° resolution National Centers for Environmental Prediction (NCEP) Climate Forecast System Reanalysis (CFSR) (Saha et al., 2010) and run until the basin-wide mean kinetic energy has reached statistical equilibrium; and 2) it is continued with 1-hourly surface NCEP CFSR wind (according to Eq. (8)) and thermal forcing from 1993 to June 2002. Both simulations used here are initialized from the ocean state at

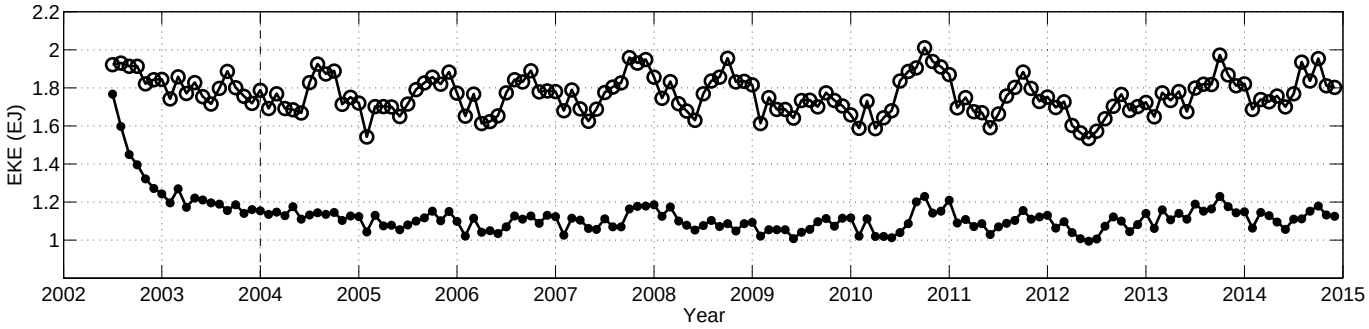

Fig. 1. Time series of the global integral of monthly EKE (EJ, 10^{18} J) relative to the monthly mean flow for experiments 1 (open circles, Eq. (8)) and 2 (solid circles, Eq. (7)). The dashed line indicates the beginning of 2004. The analysis in this study focuses on time from 2004 to 2014.

the end of June 2002 from step 2 and run for 12.5 years from July 2002 to the end of 2014. The two simulations used in this study are the same as those used in Yu et al. (2017). The mean Kuroshio transport (Fig. 1 in Yu et al., 2017) indicates that it takes 18 months for experiment 2 to adjust to the impulse associated with the new wind stress formulation (Eq. (7)) to reach to a steady state. The same conclusion can be drawn from the global integral of the monthly mean EKE (relative to the monthly mean currents) time series (Fig. 1). The monthly mean EKE in experiment 2 (line with solid circles) decreases dramatically in the first 18 months and varies slowly from 2004 onward. Thus, we focus on results of the last 11 years, 2004 to 2014. Daily averages of u_i and ρ are stored every model day while surface currents and surface stress $\boldsymbol{\tau}$ are saved hourly. Vertical velocity w is a diagnostic variable, determined by vertically integrating the continuity equation downward from the surface.

3. Model results

3.1. Comparison with drifter observations

Fig. 2a shows the global near-surface mean VKE at 15-m derived from quality controlled Global Drifter Program (GDP) data set (Niiler, 2001; Lumpkin and Pazos, 2007) from 1979 to June 2012. The undrogued data from the GDP data set were removed by a reanalysis of drogue presence (Lumpkin and Johnson, 2013) and the quality controlled data were mapped on a $0.5^{\circ} \times 0.5^{\circ}$ longitude-latitude grid (Lumpkin et al., 2013). It clearly indicates that high near-surface VKE concentrates in the vicinity of major western boundary currents, the Antarctic Circumpolar Current (ACC) in the Southern Ocean, and the equatorial region. The 11-year (2004 to 2014) near-surface mean VKE (relative to the 11-year average currents) at 15-m from experiments 1 and 2 are shown in Fig. 2b and c, respectively. Results from experiment 2 show improvements in both the spatial patterns and the global average.

The spatial patterns of the two simulated global near-surface mean VKE are very similar to that revealed by the drifters, both show the high VKE around the major current systems and equatorial regions. The unrealistic excessive Agulhas eddy-shedding into the south Atlantic in experiment 1 (Fig. 2b) is a common artifact of the global models (Barnier et al., 2006; Thoppil et al., 2011) although the exact mechanism remains unknown. The disappearance of this excessive eddy-shedding in experiment 2 (Fig. 2c), which differs to experiment 1 only in wind stress formulation, suggests it can be attributed to surface wind stress forcing.

The average of the global near-surface mean VKE at 15-m from experiment 1 is $3.3 \times 10^{-2}\ {}^{m^2}/_{s^2}$, whereas the average from experiment 2 is $1.9 \times 10^{-2}\ {}^{m^2}/_{s^2}$. The difference, $-1.4 \times 10^{-2}\ {}^{m^2}/_{s^2}$, represents a 42% reduction due to the inclusion of ocean surface currents in the wind stress formulation and is in good agreement with previous studies (Zhai and Greatbatch, 2007; Eden and Dietze, 2009; Seo et al., 2016; Renault et al., 2016a; Renault et al., 2016b). The average of the near-surface VKE from experiment 2 is closer to the observed value of $2.2 \times 10^{-2}\ {}^{m^2}/_{s^2}$ and represents 85% of the observation while the result from experiment 1 is 51% more than the observation. Part of the difference between the numerical simulations (Fig. 2b and c) and the GDP data can be explained by the influence of the interannual to decadal variability since the start time and the time duration (34 vs 11 years) of the GDP data and numerical simulations are both different.

3.2. Depth-integrated mean VKE from 2004 to 2014

Similar to the VKE at 15-m, the depth-integrated mean VKE from the experiment 2 (Fig. 3b) during 2004–2014 is also smaller than that from experiment 1 (Fig. 3a). The global sum is 4.58 and 3.04 EJ (10^{18} J) in experiment 1 and 2, respectively. The difference, −1.54 EJ, indicates a 34% global VKE reduction due to the inclusion of ocean surface currents in the wind stress formulation. Both spatial patterns are similar to that derived from the surface drifters and the correlation is 0.92 between experiment 1 and 2. The global total VKE is estimated to be 3.8 EJ by Wunsch (1998) using current meter moorings data from Wunsch (1997). The global total VKE in experiment 1 (2) is 20% more (less) than the estimate in Wunsch (1998).

The VKE contains kinetic energy associated with the monthly mean flow variation relative to the 11-year average and the monthly EKE (Fig. 1a) associated with the eddy motions relative to the slow variation of the monthly mean flow. As mentioned in Section 1, the VKE budget is simply $0 = SP + BW + \varepsilon$, which doesn't show the time evolution of the kinetic energy. And thus, we focus on the monthly EKE in this study.

Obviously, the effect of including the ocean surface currents in the wind stress formulation reduces both the VKE and EKE. Below, we perform the domain EKE budget analysis using the monthly mean EKE time series (Fig. 1a) to study which processes lead to this reduction. The overbar terms (e.g. $\overline{u_i}$) in Eqs. (2) to (6) represent the monthly average calculated from daily average model output and the prime terms (e.g. u_i') represent the daily fluctuation relative to the monthly average. Hourly surface stress and currents are first averaged daily and then used in the calculation. The average monthly EKE during 2004–2014 is 1.10 EJ in experiment 2, which is 37% less than the average in experiment 1, 1.76 EJ (Fig. 1).

3.3. Shear production, buoyancy work, and the eddy wind work

The spatial patterns of *SP*, *BW*, the eddy wind work on ageostrophic, and geostrophic currents in August 2010 are shown as an example in Fig. 4. The spatial patterns of these terms in experiment 1 (Fig. 4a, c, e, and g) are all similar to the ones in experiment 2 (Fig. 4b, d, f, and h).

For *SP*, *BW*, and eddy wind work on geostrophic currents, most of the contributions come from the high mesoscale eddy activity regions: the major western boundary currents, equatorial region, and the ACC in the Southern Ocean. The global sum of *SP*, *BW*, and eddy wind work on

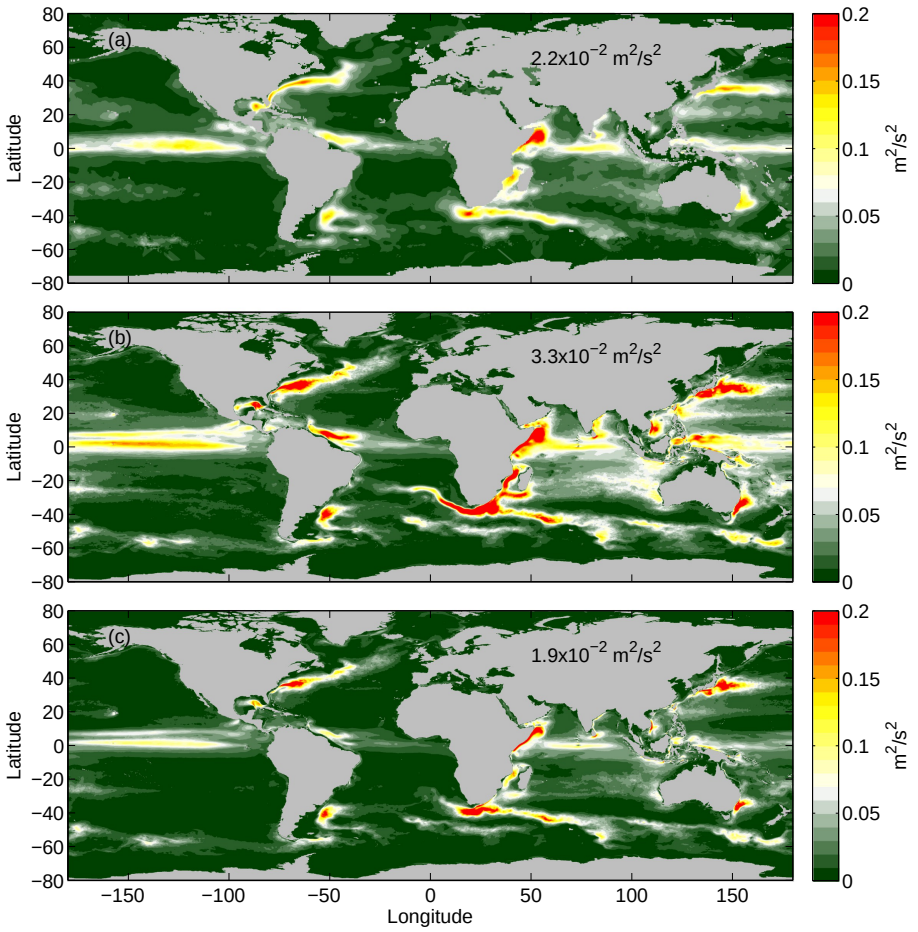

Fig. 2. The spatial patterns of the mean near surface VKE (m^2/s^2) at 15-m revealed by (a) drifter observations during 1979–2012, (b) experiment 1, and (c) experiment 2 during 2004–2014. The global average is noted over Asia.

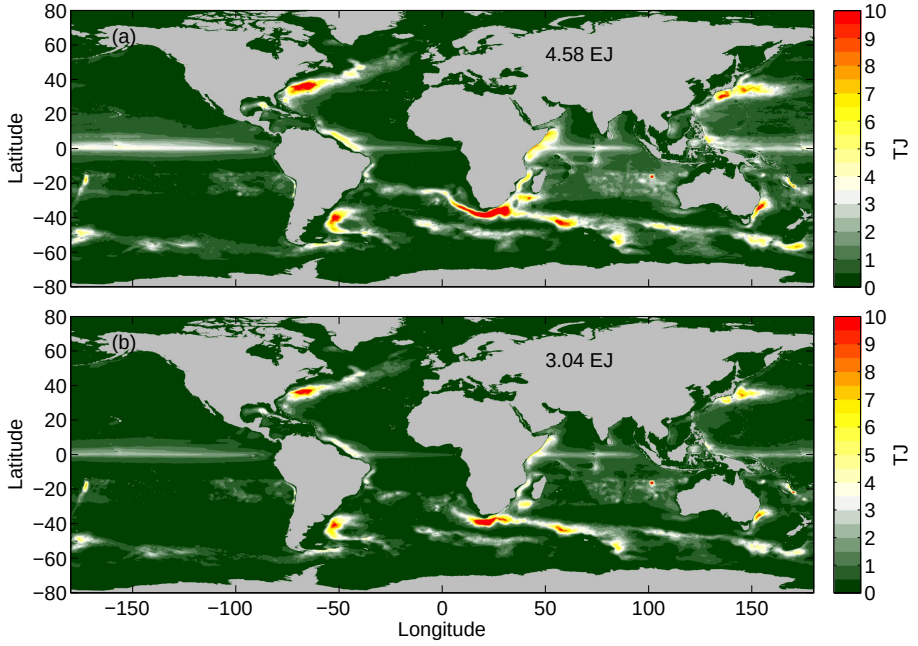

Fig. 3. The depth-integrated global mean VKE (TJ, 10^{12} J) during 2004–2014 from (a) experiment 1, and (b) experiment 2. The global sum (EJ, 10^{18} J) is noted over Asia.

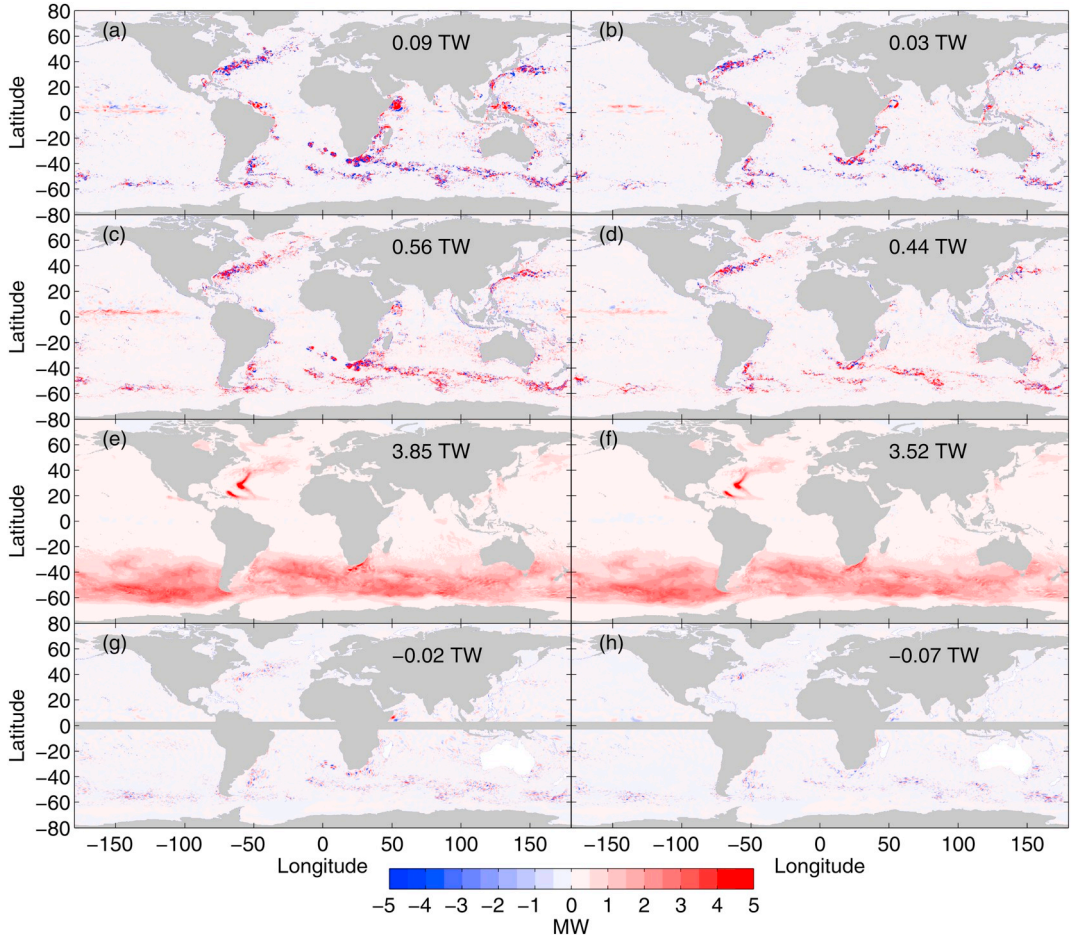

Fig. 4. The spatial patterns of *SP*, *BW*, eddy wind work on ageostrophic, and geostrophic currents (MW, 10^6 W) in August 2010 from experiment 1 (a, c, e, g), and experiment 2 (b, d, f, h), respectively. The global sum is noted over Asia.

geostrophic currents is 0.09, 0.56, −0.02 (0.03, 0.44, −0.07) TW (10^{12} W) in experiment 1 (2), respectively.

For eddy wind work on ageostrophic currents (Fig. 4e and f), most of the contributions comes from the Southern Ocean south of 40°S (Fig. 4e, f) due to the strong currents driven by strong wind stress in boreal summer. The only strong signals in the Northern Hemisphere are in North Atlantic, which are generated by major hurricanes Danielle and Earl in 2010. The global sum is 3.85 and 3.52 TW in experiment 1 and 2, respectively. These two values are much larger than the previous estimate of 1.73 TW (Wang and Huang, 2004). Wang and Huang (2004) indicated that they may underestimate the wind work on the ageostrophic currents due to: (1) the 45° angle between the wind stress and surface ageostrophic current from the classical Ekman theory is more than the observed 5° to 20° angle between wind stress and surface drifter velocity, which underestimates the surface ageostrophic current along the wind stress direction; and (2) the empirical constant γ used to calculate Ekman Depth D_e ($D_e = \gamma \frac{u_*}{f}$, where $u_*$is the frictional velocity and f is the Coriolis parameter) is chosen to be 0.5 that is higher than the commonly used values of $\gamma \approx 0.25 - 0.4$. This overestimates the Ekman depth and in turn underestimates wind work on the ageostrophic currents as indicated by Wang and Huang (2004, their Eq. (14) as shown below).

$$W_e = \sum_{-\infty}^{\infty} \frac{1}{\rho_o D_e} \left(\frac{1}{|f\,(f+\omega_n)|} \right)^{1/2} T_n^2, \tag{10}$$

where ω_n and T_n are the frequency and magnitude of the nth component of the wind stress, respectively. Previous estimates of the wind work on ageostrophic currents (Huang et al., 2006; Von Storch et al., 2007; Von Storch et al., 2012) based on numerical simulations suffer from a thicker top layer depth (5 to 30 m) than used here that underestimates the surface ageostrophic currents due to the vertical average. Detailed analysis on this aspect can be found in Yu et al. (2018).

The global sum of the four terms above shows that the magnitude of *SP* and eddy wind work on geostrophic currents is one order of magnitude smaller than *BW* and two orders of magnitude smaller than the eddy wind work on ageostrophic currents. Does this mean we should eliminate *SP*, *BW*, and eddy wind work on geostrophic currents from the domain integral of EKE analysis?

3.4. The EKE budget

Time series of $\frac{\partial(EKE)}{\partial t}$ are shown in Fig. 5a. The time series of *SP* (solid lines), *BW* (lines with dots), eddy wind work on geostrophic currents (dash-dotted lines), eddy wind work on ageostrophic currents (lines with squares), and *td* (lines with triangles) are shown in Fig. 5b. *td* is calculated as the difference between $\frac{\partial(EKE)}{\partial t}$ and the sum of *SP*, *BW*, and the eddy wind work (Eqs. (1) to (6)). Please note that the scale of y-axis in Fig. 5b from −0.75 to 0.75 is three times larger than the scale beyond the range. The smaller terms in Fig. 5b, *SP* and eddy wind work on geostrophic currents, are on the same order as $\frac{\partial(EKE)}{\partial t}$ (Fig. 5a). Thus, we should not eliminate any terms from the domain integral of EKE analysis. All of these terms are important.

In both experiments, *SP*, *BW*, and eddy wind work on ageostrophic currents are generally energy sources and *td* and eddy wind work on geostrophic currents are the energy sinks. The average of *SP*, *BW*, eddy wind work on ageostrophic currents, eddy wind work on geostrophic

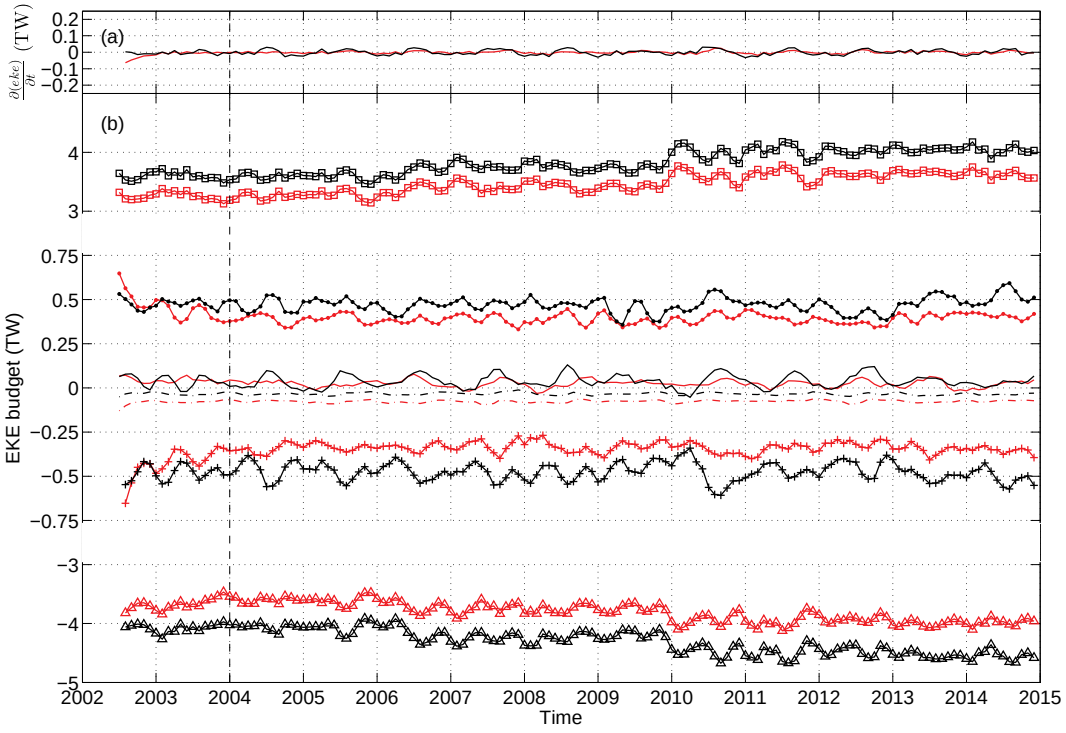

Fig. 5. Time series of (a) $\frac{\partial(EKE)}{\partial t}$ (TW, 10^{12} W), and (b) eddy wind work on ageostrophic currents (lines with squares, $\int_S \overline{\tau' \cdot V'_{ag}} dS$), *BW* (lines with dots), *SP* (solid lines), eddy wind work on geostrophic currents (dash-dotted lines, $\int_S \overline{\tau' \cdot V'_g} dS$), ε_{ag} ($\int_S \overline{\tau' \cdot V_{ag}'} dS + td$, lines with plus), and *td* (lines with triangles) for experiments 1 (black) and 2 (red). Please note that the scale of y-axis in Fig. 5b from −0.75 to 0.75 is three times larger than the scale beyond the range. The dashed line indicates the beginning of 2004. The analysis in this study focuses on time from 2004 to 2014. (For interpretation of the references to color in this figure legend, the reader is referred to the web version of this article.)

Table 1
The average (TW, 10^{12} W) of the shear production (*SP*), buoyancy work (*BW*), eddy wind work on ageostrophic ($\overline{\tau' \cdot V'_{ag}}$) and geostrophic currents ($\overline{\tau' \cdot V'_g}$), and the sub-surface turbulence dissipation (*td*) during the steady state (2004–2014). Experiment 1 does not include the effect of ocean surface currents in the wind stress formulation whereas experiment 2 does.

EKE term	*SP*	*BW*	$\overline{\tau' \cdot V'_{ag}}$	$\overline{\tau' \cdot V'_g}$	*td*
Experiment 1	0.04	0.47	3.84	−0.03	−4.32
Experiment 2	0.02	0.39	3.48	−0.07	−3.82
Magnitude change	−37%	−17%	−9%	130%	−12%

currents, and *td* during 2004–2014 in experiment 1 (black lines) are 0.04, 0.47, 3.84, −0.03, and, −4.32 TW (Table 1), respectively. The corresponding averages in experiment 2 (red lines) are 0.02, 0.39, 3.48, −0.07, and −3.82 TW (Table 1), respectively. The magnitudes of *SP*, *BW*, eddy wind work on ageostrophic currents, and *td* in the last 11 years (2004–2014) are reduced by 37%, 17%, 9%, and 12% (Table 1), respectively when ocean surface currents are included in the surface stress formulation (Eq. (7)). The magnitude of the eddy wind work on geostrophic currents, on the other hand, increases by 130%.

As mentioned in section 1, the eddy wind work on ageostropchic currents is fully dissipated by the turbulence in the upper ocean mixed layer. Thus, the eddy wind work on ageostrophic currents and *td* is combined together as ε_{ag} and is also shown in Fig. 5b (line with plus symbols). The average of ε_{ag} during 2004–2014 is −0.48 (−0.34) TW, in the same order as *BW*, in experiment 1 (2). Its magnitude is reduced by 27% when ocean surface currents are included in the surface stress formulation.

3.5. Budget of EKE difference

Instead of analyzing the EKE budget for the individual experiments, we now analyze the budget of EKE difference between the two experiments to reveal what causes the reduction of the EKE

$$\frac{\partial(EKE_d)}{\partial t} = SP_d + BW_d + \overline{\tau' \cdot V'_g}_d + \varepsilon_{agd}, \tag{11}$$

where the subscript *d* is defined as the difference between experiment 2 and 1, i.e.

$$EKE_d = EKE_2 - EKE_1. \tag{12}$$

The time series of all five terms in Eq. (11) are shown in Fig. 6a. The averages of SP_d (blue line), BW_d (green line), and $\overline{\tau' \cdot V'_g}_d$ during 2004–2014 are negative, −0.01, −0.08, and −0.04 TW respectively, which indicates that they are responsible for the EKE reduction when ocean surface currents are included in the wind stress formulation and they are in the same order of magnitude. Quantitatively, the most dominant term is BW_d, and then $\overline{\tau' \cdot V'_g}_d$, with SP_d the least important. The average of ε_{agd} (black dashed line) in the same period is positive, 0.13 TW to balance the budget.

3.6. The transition period

The surface stress formulation in experiment 2 includes ocean surface currents, which is different from how the initialization state was generated. Thus, the simulated global ocean in experiment 2 has to adjust to the impulse associated with the new wind stress formulation through both barotropic and baroclinic adjustments. And there exists an obvious downward (upward) linear trend in BW_d (ε_{agd}) (Fig. 6a) from July 2002 to December 2003.

The impulse associated with the new wind stress formulation provides an additional energy source for baroclinic instability via the

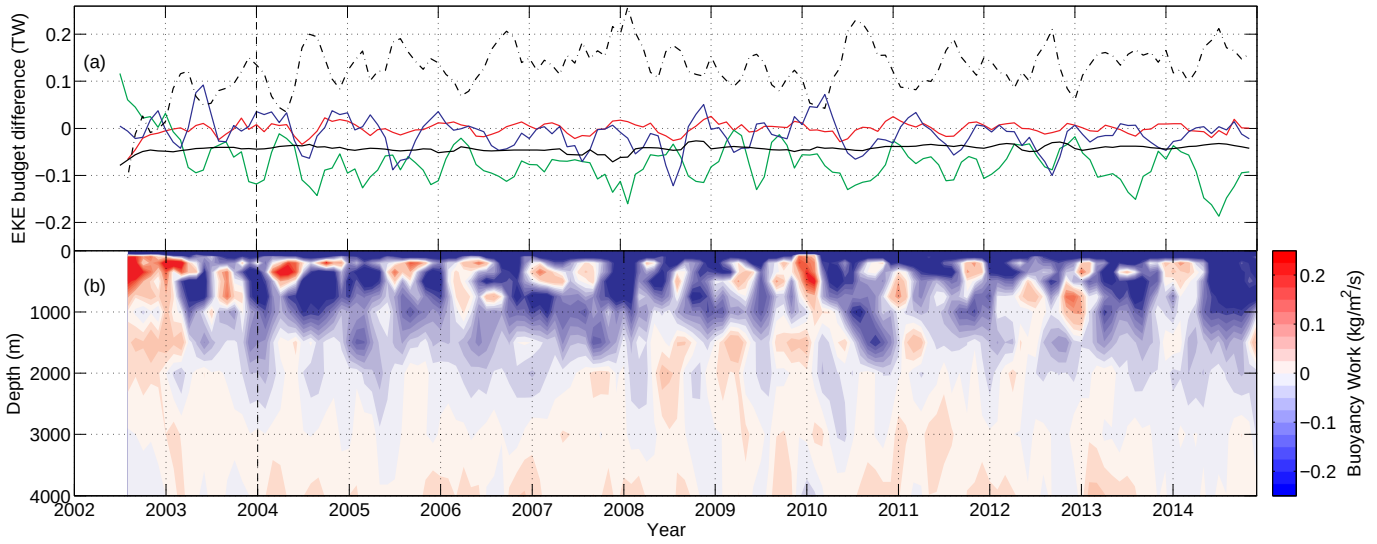

Fig. 6. Time series of (a) $\frac{\partial(eke_d)}{\partial t}$ (red, TW, 10^{12} W), SP_d (blue), BW_d (green), $\overline{\tau' \bullet V'_g}_d$ (black solid), and ε_{agd} (black dash-dotted); and (b) the vertical profile of BW_d averaged across the globe. The subscript d is defined as the difference between experiment 2 and 1. The dashed line indicates the beginning of 2004. The analysis in this study focuses on time from 2004 to 2014. (For interpretation of the references to color in this figure legend, the reader is referred to the web version of this article.)

baroclinic adjustments in experiment 2. Thus, BW in experiment 2 is larger than that in experiment 1 at the beginning of the simulation (Fig. 5b, lines with dots) and the BW_d is positive (Fig. 6a, green line). The EKE in the upper ocean associated with baroclinic instability is transferred down to the abyssal ocean through the nonlinear interaction between the barotropic and baroclinic flow (Rhines, 1979; Salmon, 1998; Haney et al., 2001). A time series of the vertical profile of BW_d is shown in Fig. 6b. It indicates that the first beam of positive BW_d in the upper ocean is transferred downward and reaches abyssal ocean in February 2003. The result of this process is the conversion between the EKE associated with baroclinic and barotropic instability (Haney et al., 2001). The BW_d and SP_d are significantly correlated with a correlation coefficient of -0.24, and the negative correlation agrees with Haney et al. (2001).

Barotropic adjustment, on the other hand, is almost instantaneous. The magnitude of td in experiment 2 reduces as compared with experiment 1 at the beginning of the simulation to respond to the eddy wind work reduction (Fig. 5b, red line with triangle). But the magnitude of td reduction is smaller than the reduction of the eddy wind work on ageostrophic currents at that time and thus the ε_{ag} in experiment 2 (Fig. 5b, red line with plus) is smaller than that in experiment 1 and the ε_{agd} is negative (Fig. 6a, black dashed line). As the baroclinic EKE is gradually transferred downward, the deeper ocean is impacted by the baroclinic adjustments. The magnitude of td reduces further and eventually exceeds the reduction of the eddy wind work on ageostrophic currents and ε_{agd} becomes positive from February 2003 (Fig. 6a). And when the ocean is fully baroclinically adjusted, ε_{agd} becomes the energy source for the budget of the EKE difference.

The dominant process in the transition period is the reduction of wind work on geostrophic currents, $\overline{\tau' \bullet V'_g}_d$, with a global sum of -0.05 TW (Table 2). The secondary contribution comes from the reduction of buoyancy work, BW_d, -0.02 TW. The contribution from the difference of SP is negligible.

Table 2
The average (TW, 10^{12} W) of the difference of the shear production (SP_d), buoyancy work (BW_d), eddy wind work on geostrophic ($\overline{\tau' \bullet V'_g}_d$) and ε_{agd} during the transition period (July 2002–December 2003). Subscript d is defined as the difference between experiment 2 and 1.

EKE_d term	SP_d	BW_d	$\overline{\tau' \bullet V'_g}_d$	ε_{agd}
	0.00	−0.02	−0.05	0.05

4. Discussion and conclusions

In this study, we investigate the impact of ocean surface currents on global EKE via the wind stress formulation. Two HYCOM numerical simulations were run for a 12.5-year period (from July 2002 to 2014) with (Experiment 2) and without (Experiment 1) ocean currents in the wind stress formulation. Both numerical simulations are in steady state in the last 11 years (2004–2014). The model results indicate that the average monthly global EKE in the steady state is reduced by 37% when ocean currents are included in the surface wind stress formulation.

A monthly EKE budget is performed for both experiments. The most dominant terms are eddy wind work on ageostrophic currents ($\overline{\tau' \bullet V'_{ag}}$) and the sub-surface turbulence dissipation (td). Since the eddy wind work on ageostrophic currents is fully dissipated in the upper ocean mixed layer, we combine these two terms as ε_{ag}. Both EKE budgets indicate that the shear production (SP) and buoyancy work (BW) are EKE sources and the ε_{ag} and the eddy wind work on geostrophic currents ($\overline{\tau' \bullet V'_g}$) are the EKE sink terms. In the steady state, SP, BW, and the eddy wind work on geostrophic currents are all reduced by the inclusion of the surface currents into the wind stress formulation and are all responsible for the monthly EKE reduction. The budget of the monthly EKE difference reveals that the primary contribution of EKE reduction comes from the reduction of BW, followed by the reduction of the eddy wind work on geostrophic currents and SP.

4.1. Kinetic energy of the mean currents

The depth-integrated kinetic energy of the mean currents, averaged over 2004–2014, is shown in Fig. 7. Strong kinetic energy of the mean currents concentrates in major western boundary currents, the ACC in the Southern Ocean, and the equatorial currents. The global sum is 1.79 and 1.49 EJ in experiment 1 (Fig. 7a) and 2 (Fig. 7b), respectively. This represents a 17% reduction due to the inclusion of the surface currents into the wind stress formulation. Part of this reduction comes from the reduced transport of the western boundary currents when the surface currents are included into the wind stress formulation (Yu et al., 2017).

The kinetic energy of the mean currents forms sharp and narrow

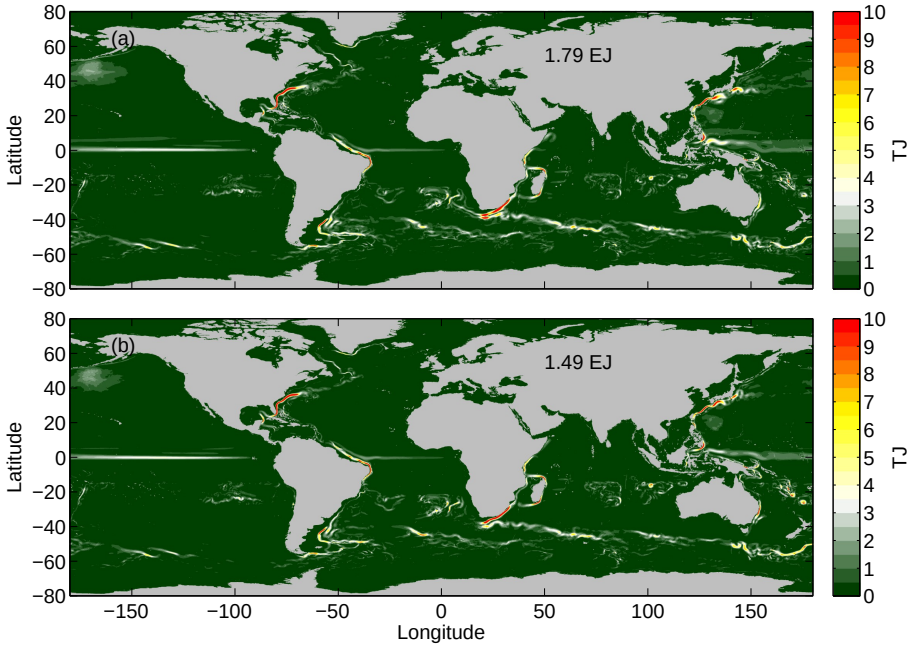

Fig. 7. The depth-integrated global kinetic energy (TJ, 10^{12} J) of the mean flow during 2004–2014 from (a) experiment 1, and (b) experiment 2. The global sum (EJ, 10^{18} J) is noted over Asia.

fine structures along the major current systems, while the spatial pattern of VKE (Fig. 3) is much smoother and broader. This reveals that the main path of the major currents varies little over time. The global sum of the kinetic energy of the mean currents is much smaller than the sum of VKE. Both of these points agree well with Von Storch et al. (2012).

4.2. Why global sum of SP is smaller than BW

Comparing *SP*, *BW*, and eddy wind work in Fig. 4, it's clear that *SP* can be the most dominant term locally. The reanalysis results show that only four terms among the nine terms in *SP* are important, which is the same as Eden and Boning (2002). These four terms are $-\rho_o \int_V \overline{u'u'}\frac{\partial \bar{u}}{\partial x}dV$, $-\rho_o \int_V \overline{v'v'}\frac{\partial \bar{v}}{\partial y}dV$, $-\rho_o \int_V \overline{u'v'}\frac{\partial \bar{u}}{\partial y}dV$, and $-\rho_o \int_V \overline{u'v'}\frac{\partial \bar{v}}{\partial x}dV$. The sum of the first two terms is $-\rho_o \int_V (\overline{u'u'} - \overline{v'v'})\frac{\partial \bar{u}}{\partial x}dV$ after applying mass conservation, that is smaller than either of the two individual terms. From the left side to the right side of the major current systems, both $\frac{\partial \bar{u}}{\partial y}$ and $\frac{\partial \bar{v}}{\partial x}$ change sign and the third and fourth terms above tend to balance across the major current systems. Thus, the global sum of *SP* is smaller.

4.3. How to improve the VKE simulation

As mentioned in sections 3.1 and 3.2, experiment 2 does a better job in simulating both the surface and total VKE than experiment 1. It also indicates that results in experiment 2 underestimate the surface and total VKE. To achieve an even more realistic simulation, one can increase the model resolution. The VKE in a non-data assimilative numerical simulation is generated by the intrinsic instability. Increasing model resolution in experiment 2 can better resolve the sub-mesoscale eddies and thus increase the mean current shear, enhance the instability, and boost the VKE (Thoppil et al., 2011). Another method is data assimilation, in which the realistic eddies are introduced by assimilating remotely sensed sea surface height data.

The ocean and the atmosphere are a fully coupled system. By comparing results from an uncoupled and coupled ocean-atmosphere simulations, Renault et al. (2016a) demonstrated that the VKE reduction due to the inclusion of surface currents in wind stress formulation is overestimated when not considering the feedback of ocean surface currents on the wind simulations in the atmospheric model. The feedback of the ocean surface currents on the wind itself through wind stress opposes the effect of the ocean surface currents on the surface stresses and can partly reenergize the ocean. According to Renault et al. (2016a), the fully coupled global ocean-atmosphere models should increase the VKE in experiment 2.

Acknowledgments

The authors thank the editor and the anonymous reviewers for their input to improve the original manuscript. Financial support for Z. Yu is provided by Karle's Research Fellowship, Naval Research Laboratory, DC. E. J. Metzger is funded by the "6.1 Kuroshio and Ryukyu Current Dynamics" project sponsored by the Office of Naval Research under program element 0601135N. Computer time was provided by the Department of Defense (DoD) High Performance Computing Modernization Program and the simulations were performed on the Cray XC30 (Shepard) at the Navy DoD Supercomputing Resources Center, Stennis Space Center, MS. The output used in the research can be provided upon individual request. This is NRL contribution NRL/JA/7320-17-3543. It has been approved for public release and distribution is unlimited.

References

Barnier, B., et al., 2006. Impact of partial steps and momentum advection schemes in a global ocean circulation model at eddy-permitting resolution. Ocean Dyn. 56, 543–567. https://doi.org/10.1007/s10236-006-0082-1.

Bleck, R., 2002. An oceanic general circulation model framed in hybrid isopycnic-Cartesian coordinates. Ocean Model 4, 55–88.

Dawe, J.T., Thompson, L., 2006. Effect of ocean surface currents on wind stress, heat flux, and wind power input to the ocean. Geophys. Res. Lett. 33, L09604. https://doi.org/10.1029/2006GL025784.

Duhaut, T.H.A., Straub, D.N., 2006. Wind stress dependence on ocean surface velocity: implications for mechanical energy input to ocean circulation. J. Phys. Oceanogr. 36, 202–211.

Eden, C., Boning, C., 2002. Sources of eddy kinertic energy in the Labrador Sea. J. Phys. Oceanogr. 32, 3346–3363.

Eden, C., Dietze, H., 2009. Effects of mesoscale eddy/wind interactions on biological new production and eddy kinetic energy. J. Geophys. Res. 114, C05023. https://doi.org/10.1029/2008JC005129.

Ferrari, R., Wunsch, C., 2009. Ocean circulation kinetic energy: reservoirs, sources and sinks. Annu. Rev. Fluid Mech. 41, 253–282. https://doi.org/10.1146/annurev.fluid.

40.111406.102139.
Ferrari, R., Wunsch, C., 2010. The distribution of eddy kinetic and potential energies in the global ocean. Tellus, Ser. A 62, 92–108.
Haney, R.L., Hale, R.A., Dietrich, D.E., 2001. Offshore propagation of eddy kinetic energy in the California current. J. Geophys. Res. 106, 11709–11717.
Holland, W., Harrison, D.E., Semtner, A.J., 1983. Eddy resolving general circulation models. In: Robinson, A.R. (Ed.), Eddies in Marine Science. Springer-Verlag, New York.
Huang, R.X., Wang, W., Liu, L.L., 2006. Decadal variability of wind-energy input to the world ocean. Deep-Sea Res. II 53, 31–41. https://doi.org/10.1016/j.dsr2.2005.11.001.
Hughes, C.W., Wilson, C., 2008. Wind work on the geostrophic ocean circulation: an observational study of the effect of small scales in the wind stress. J. Geophys. Res. 113, C02016. https://doi.org/10.1029/2007JC004371.
Hughes, G.O., Hogg, A.McC., Griffiths, R.W., 2009. Available potential energy and irreversible mixing in the meridional overturning circulation. J. Phys. Oceanogr. 39, 3130–3146. https://doi.org/10.1175/2009JPO4162.1.
Kelly, K.A., Dickinson, S., McPhaden, M.J., Johnson, G.C., 2001. Ocean currents evident in satellite wind data. Geophys. Res. Lett. 28, 2469–2472.
Kuhlbrodt, T., Griesel, A., Montoya, M., Levermann, A., Hofmann, M., Rahmstorf, S., 2007. On the driving processes of the Atlantic meridional overturning circulation. Rev. Geophys. 45, RG2001. https://doi.org/10.1029/2004RG000166.
Lumpkin, R., Johnson, G.C., 2013. Global ocean surface velocities from drifters: mean, variance, El Nino-southern oscillation response, and seasonal cycle. J. Geophys. Res. 118, 2992–3006. https://doi.org/10.1002/jgrc.20210.
Lumpkin, R., Pazos, M., 2007. Measuring surface currents with surface velocity program drifters: the instrument, its data and some recent results. In: Griffa, A. (Ed.), Lagrangian Analysis and Prediction of Coastal and Ocean Dynamics. Cambridge Univ. Press, Cambridge, pp. 39–67 chap. 2.
Lumpkin, R., Grodsky, S., Centurioni, L., Rio, M.-H., Carton, J., Lee, D., 2013. Removing spurious low-frequency variability in drifter velocities. J. Atmos. Ocean. Technol. 30, 353–360. https://doi.org/10.1175/JTECH-D-12-00139.1.
Luo, J.-J., Masson, S., Roeckner, R., Madec, G., Yamagata, T., 2005. Reducing climatology bias in an ocean-atmosphere CGCM with improved coupling physics. J. Clim. 18, 2344–2360.
Niiler, P. P., 2001. The world ocean surface circulation. in Ocean Circulation and Climate, Int. Geophys. Ser., vol. 77, edited by G. Siedler, J. Church, and J. Gould, pp. 193–204, Academic Press, San Diego, Calif.
Pacanowski, R.C., 1987. Effect of equatorial currents on surface stress. J. Phys. Oceanogr. 17, 833–838.
Renault, L., Molemaker, M.J., McWilliams, J.C., Shchepetkin, A.F., Lemarie, F., Chelton, D., Illig, S., Hall, A., 2016a. Modulation of wind work by oceanic current interaction with the atmosphere. J. Phys. Oceanogr. 46, 1685–1704. https://doi.org/10.1175/JPO-D-15-0232.1.
Renault, L., Molemaker, M.J., Gula, J., Masson, S., McWilliams, J.C., 2016b. Control and stabilization of the Gulf Stream by oceanic current interaction with the atmosphere. J. Phys. Oceanogr. 46, 3439–3453. https://doi.org/10.1175/JPO-D-16-0115.1.
Rhines, P.B., 1979. Geostrophic turbulence. Annu. Rev. Fluid Mech. 11, 401–444.
Richardson, P.L., 1983. Eddy kinetic energy in the North Atlantic from surface drifters. J. Geophys. Res. 88 (C7), 4355–4367.
Saha, S., et al., 2010. The NCEP climate forecast system reanalysis. Bull. Amer. Meteor. Soc. 91, 1015–1057. https://doi.org/10.1175/2010BAMS3001.1.
Salmon, R., 1998. Lectures on Geophysical Fluid Dynamics. 378 pp. Oxford Univ. Press, New York.
Seo, H., Miller, A.J., Norris, J.R., 2016. Eddy-wind interaction in the California Current System: dynamics and impacts. J. Phys. Oceanogr. 46, 439–459. https://doi.org/10.1175/JPO-D-15-0086.1.
Stammer, D., 1997. Global characteristics of ocean variability estimated from regional TOPEX/POSEIDON altimeter measurements. J. Phys. Oceanogr. 27, 1743–1769.
Thoppil, P.G., Richman, J.G., Hogan, P.J., 2011. Energetics of a global ocean circulation model compared to observations. Geophys. Res. Lett. 38. https://doi.org/10.1029/2011GL048347.
Von Storch, J.S., Sasaki, H., Marotzke, J., 2007. Wind-generated power input to the deep ocean: an estimate using a 1/10° general circulation model. J. Phys. Oceanogr. 37. https://doi.org/10.1175/JPO3001.1.
Von Storch, J.S., Eden, C., Fast, I., Haak, H., Hernandez-Deckers, D., Maier-Reimer, E., Marotzke, J., Stammer, D., 2012. An estimate of the Lorenz energy cycle for the world ocean based on 1/10° STORM/NCEP simulation. J. Phys. Oceanogr. 42. https://doi.org/10.1175/JPO-D-12-079.1.
Wang, W., Huang, R.X., 2004. Wind energy input to the Ekman layer. J. Phys. Oceanogr. 34, 1267–1275.
Wunsch, C., 1997. The vertical partition of oceanic horizontal kinetic energy. J. Phys. Oceanogr. 27, 1770–1794.
Wunsch, C., 1998. The work done by the wind on the oceanic general circulation. J. Phys. Oceanogr. 28, 2332–2340.
Xu, Y., Scott, R.B., 2008. Subtleties in forcing eddy resolving ocean models with satellite wind data. Ocean Model 20, 240–251. https://doi.org/10.1016/j.ocemod.2007.09.003.
Yu, Z., Metzger, E.J., Fan, Y., 2017. The impact of ocean surface currents on Sverdrup transport in the midlatitude North Pacific via the wind stress formulation. J. Phys. Oceanogr. 47. https://doi.org/10.1175/JPO-D-16-0155.1.
Yu, Z., Fan, Y., Metzger, E.J., Smedstad, O.M., 2018. The wind work input into the global ocean revealed by a 17-year global HYbrid Coordinate Ocean Model reanalysis. Ocean Model. https://doi.org/10.1016/j.ocemod.2018.07.009.
Zhai, X., Greatbatch, R.J., 2007. Wind work in a model of the Northwest Atlantic Ocean. Geophys. Res. Lett. 34, L04606. https://doi.org/10.1029/2006GL028907.